Equation of states and transport properties of warm dense beryllium: A quantum molecular dynamics study

Cong Wang,[1,2] Yao Long,[1] Ming-Feng Tian,[1] Xian-Tu He,[1,2] and Ping Zhang[1,2,*]

[1]*Institute of Applied Physics and Computational Mathematics, P.O. Box 8009, Beijing 100088, People's Republic of China*

[2]*Center for Applied Physics and Technology, Peking University, Beijing 100871, People's Republic of China*

Abstract

We have calculated the equation of states, the viscosity and self-diffusion coefficients, and electronic transport coefficients of beryllium in the warm dense regime for densities from 4.0 to 6.0 g/cm^3 and temperatures from 1.0 to 10.0 eV by using quantum molecular dynamics simulations. The principal Hugoniot is accordant with underground nuclear explosive and high power laser experimental results up to $\sim$ 20 Mbar. The calculated viscosity and self-diffusion coefficients are compared with the one-component plasma model, using effective charges given by the average-atom model. The Stokes-Einstein relationship, which presents the relationship between the viscosity and self-diffusion coefficients, is found to hold fairly well in the strong coupling regime. The Lorenz number, which is the ratio between thermal and electrical conductivities, is computed via Kubo-Greenwood formula and compared to the well-known Wiedemann-Franz law in the warm dense region.

PACS numbers: 64.30.-t, 66.20.-d, 72.15.Cz

*Corresponding author: zhang_ping@iapcm.ac.cn

I. INTRODUCTION

The nature of compressed matter is of considerable interest for many fields of modern physics, including astrophysics [1], inertial confinement fusion (ICF) [2, 3], and other related fields [4]. Materials under a pressure greater than a few Mbar can be drived into a strongly coupled, partially ionized fluid states, which is defined as the so-called warm dense matter (WDM). Theoretical modeling and experimental detection of the high pressure behavior of WDM are of great challenge and are being in extensive investigations. Among various kinds of WDMs, warm dense beryllium (Be) is of particular current interest. The equation of states (EOS) and transport properties of Be are very important in ICF, due to its appearance in the ablator of Deuterium-Tritium (D-T) capsule. The compressibility of the capsule, laser absorption, and instability growth at the fuel-ablator interface sensitively depend on the thermo-physical properties of Be [5].

The EOS of Be at shock Hugoniot up to ~ 18 Mbar have been accessed by strong shock waves generated by underground nuclear explosives [6, 7]. Then, it is also possible to probe similar pressure range in the laboratory by high intensity laser [8]. Despite the success of these techniques in detecting wide range EOS of typical matters, one should note that after several decades, only seven Hugoniot points are available for Be, and more experimental data are desired for building successful theoretical models, such as interatomic potentials or chemical models currently used in SESAME EOS [9]. As another parameter in determining the EOS, temperature, which is difficult to be measured in nuclear explosion or high power laser experiments, is still needed to be clarified. Apart from the EOS, the atomic diffusion coefficients and fluid viscosity are key ingredients to control hydrodynamic instabilities near interfaces [10–12]. The electronic dynamic conductivity, from which dielectric function can be obtained, determines a series of interactions between laser and matters [13, 14]. Due to these key issues to be addressed, therefore, the thermo-physical properties of Be in the warm dense region are highly recommended to be understood in a systematic and self-consistent way.

In the present work, quantum molecular dynamics (QMD) simulations [15, 16], where electrons are fully quantum mechanically treated by finite-temperature density functional theory (FT-DFT), have been introduced to study warm dense Be. The EOS are extracted from a series of NVT assemble sampling over different densities and temperatures, then the

Hugoniot curve is calculated from the Rankine-Hugoniot relation. The self-diffusion coefficient and viscosity have been computed from the trajectory by the velocity and the stress tensor autocorrelation function. The dynamic conductivity, from which the DC conductivity and electronic thermal conductance are derived, has been obtained from Kubo-Greenwood formula. The rest of the paper is organized as follows: In Sec. II, we briefly describe the QMD simulations and computational method in determining the atomic transport properties and electronic dynamic conductivity; In Sec. III, discussions are presented for the EOS and transport properties; And In Sec. IV, we get our conclusions.

II. COMPUTATIONAL METHOD

A. Quantum Molecular Dynamics

Our QMD simulations employed the Vienna ab initio Simulation Package (VASP) [17, 18]. A series of volume fixed supercells including N atoms, which are repeated periodically throughout the space, form the elements of our calculations. After Born-Oppenheimer approximation, electrons are quantum mechanically treated through plane-wave FT-DFT. The interaction between electron and ion is presented by a projector augmented wave (PAW) pseudopotential. The exchange-correlation functional is determined within Perdew-Burke-Ernzerhof generalized gradient approximation. The ions move classically according to the forces from the electron density and the ion-ion repulsion. The system is kept in local thermodynamic equilibrium with the electron and ion temperatures equal ($T_e = T_i$). The electronic temperature is kept through Fermi-dirac distribution of the electronic states, and the ion temperature is secured through Nosé-Hoover thermostat [19].

We have chosen 216 atoms in the unit cell with periodic boundary condition. A range of densities from $\rho = 1.84$ g/cm^3 to 6.0 g/cm^3 and temperatures from $T = 300$ K to $T = 120000$ K are selected to highlight the principle Hugoniot regions. The convergence of the thermodynamic quantities plays an important role in the accuracy of QMD simulations. In the present work, a plane-wave cutoff energy of 800 eV is employed in all simulations so that the pressure is converged within 2%. We have also checked the convergence with respect to a systematic enlargement of the **k**-point set in the representation of the Brillouin zone. The correction of higher-order **k** points on the EOS data is slight and negligible. In the

molecular dynamics simulations, only Γ point of the Brillouin zone is included, while 4 × 4 × 4 Monkhorst-Pack scheme grid points are used in the electronic structure calculations. The dynamic simulations have lasted 10 ∼ 20 ps with time steps of 0.5 ∼ 1.0 fs according to different conditions. For each pressure and temperature, the system is equilibrated within 1 ∼ 2 ps. The EOS data are obtained by averaging over the final 5 ps molecular dynamic simulations.

B. Transport properties

The self-diffusion coefficient D can either be calculated from the trajectory by the mean-square displacement

$$D = \frac{1}{6t}\langle |R_i(t) - R_i(0)|^2 \rangle, \tag{1}$$

or by the velocity autocorrelation function

$$D = \frac{1}{3}\int_0^\infty \langle V_i(t) \cdot V_i(0) \rangle dt, \tag{2}$$

where R_i is the position and V_i is the velocity of the ith nucleus. Only in the long-time limit, these two formulas of D are formally equivalent. Sufficient lengths of the trajectories have been generated to secure contributions from the velocity autocorrelation function to the integral is zero, and the mean mean-square displacement away from the origin consistently fits to a straight line. The diffusion coefficient obtained from these two approaches lie within 1 % accuracy of each other, here, we report the results from velocity autocorrelation function.

The viscosity

$$\eta = \lim_{t\to\infty} \bar{\eta}(t), \tag{3}$$

has been computed from the autocorrelation function of the off-diagonal component of the stress tensor [20]

$$\bar{\eta}(t) = \frac{V}{k_B T}\int_0^t \langle P_{12}(0) P_{12}(t') \rangle dt'. \tag{4}$$

The results are averaged from the five independent off-diagonal components of the stress tensor P_{xy}, P_{yz}, P_{zx}, $(P_{xx} - P_{yy})/2$, and $(P_{yy} - P_{zz})/2$.

Different from the self-diffusion coefficient, which involves single-particle correlations and attains significant statistical improvement from averaging over the particles, the viscosity depends on the entire system and thus needs very long trajectories so as to gain statistical

accuracy. To shorten the length of the trajectory, we use empirical fits [21] to the integrals of the autocorrelation functions. Thus, extrapolation of the fits to $t \to \infty$ can more effectively determine the basic dynamical properties. Both of the D and $\bar{\eta}$ have been fit to the functional in the form of $A[1 - \exp(-t/\tau)]$, where A and τ are free parameters. Reasonable approximation to the viscosity can be produced from the finite time fitting procedure, which also serves to damp the long-time fluctuations.

The fractional statistical error in calculating a correlation function C for molecular-dynamics trajectories [22] can be given by

$$\frac{\triangle C}{C} = \sqrt{\frac{2\tau}{T_{traj}}}, \tag{5}$$

where τ is the correlation time of the function, and T_{traj} is the length of the trajectory. In the present work, we generally fitted over a time interval of $[0,\, 4\tau - 5\tau]$.

C. Dynamic Conductivity

The key to evaluate the electrical transport properties is the kinetic coefficients. They are calculated using the following Kubo-Greenwood formulation:

$$\hat{\sigma}(\epsilon) = \frac{1}{\Omega} \sum_{k,k'} |\langle \psi_k | \hat{v} | \psi_{k'} \rangle|^2 \delta(\epsilon_k - \epsilon_{k'} - \epsilon), \tag{6}$$

where $\langle \psi_k | \hat{v} | \psi_{k'} \rangle$ are the velocity matrix elements, Ω is the volume of the supercell, and ϵ_k are the electronic eigenvalues. The kinetic coefficients $\mathcal{L}_{ij}$ in the Chester-Thellung version [23] are given by

$$\mathcal{L}_{ij} = (-1)^{i+j} \int d\epsilon \hat{\sigma}(\epsilon)(\epsilon - \mu)^{(i+j-2)}(-\frac{\partial f(\epsilon)}{\partial \epsilon}), \tag{7}$$

where μ is the chemical potential and $f(\epsilon)$ is the Fermi-Dirac distribution function. The electrical conductivity σ is obtained as

$$\sigma = \mathcal{L}_{11}, \tag{8}$$

and electronic thermal conductivity K is

$$K = \frac{1}{T}(\mathcal{L}_{22} - \frac{\mathcal{L}_{12}^2}{\mathcal{L}_{11}}), \tag{9}$$

where T is the temperature. Equations (8) and (9) are energy-dependent, then the electrical conductivity and electronic thermal conductivity are obtained through extrapolating to zero

energy. In order to get converged transport coecients, ten independent snapshots, which are selected during one molecular dynamic simulation at given conditions, are selected to calculate electrical conductivity and electronic thermal conductivity as running averages.

III. RESULTS AND DISCUSSION

A. The equation of states

TABLE I: Expansion coefficients A_{ij} for the internal energy E (eV/atom).

$A_{i,j}$	$j=0$	$j=1$	$j=2$
$i=0$	0.4369	0.5386	0.3149
$i=1$	-0.7316	1.1936	-0.1149
$i=2$	0.3215	-0.1241	0.0117

TABLE II: Expansion coefficients B_{ij} for pressure P (GPa).

$B_{i,j}$	$j=0$	$j=1$	$j=2$
$i=0$	-17.9930	10.2237	-0.7659
$i=1$	-62.4972	24.4101	0.3885
$i=2$	38.7063	-0.2107	-0.0218

Wide range EOS (ρ from 4.0 to 6.0 g/cm^3 and temperatures of $1 \sim 10$ eV) have been calculated according to QMD simulations, and the internal energy E (eV/atom) and pressure P (GPa) are fitted by expansions in terms of density (g/cm^3) and temperature (eV) as follows:

$$E = \sum A_{ij} \rho^i T^j, \tag{10}$$

$$P = \sum B_{ij} \rho^i T^j. \tag{11}$$

The fitted coefficient for $A_{i,j}$and $B_{i,j}$ are summarized in Tables I and II. Here, the internal energy E at 1.84 g/cm^3 and $T = 300$ K has been taken as zero.

Based on the fitted EOS, the principal Hugoniot curve can be derived from the Rankine-Hugoniot equation, which is the locus of points in (E, P, V)-space satisfying the condition

$$(E_0 - E_1) + \frac{1}{2}(V_0 - V_1)(P_0 + P_1) = 0, \tag{12}$$

where the subscripts 0 and 1 denote the initial and shocked state, respectively. This relation follows from conservation of mass, momentum, and energy for an isolated system compressed by a pusher at a constant velocity. In the canonical (NVT) ensemble in which both E and P are temperature dependent, the locus of states which satisfies Eq. (12) is the so-called principal Hugoniot, which describes the shock adiabat between the initial and final states.

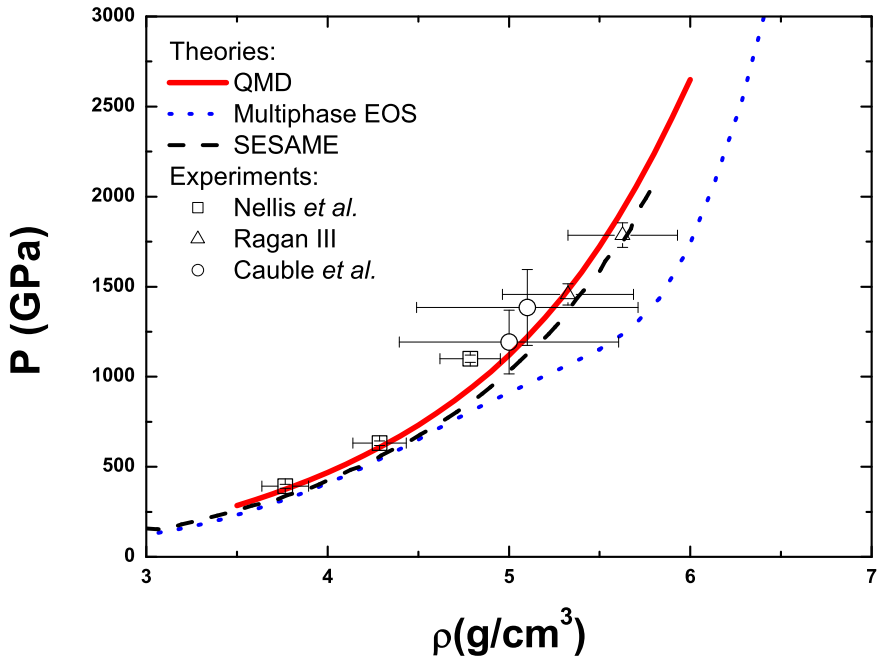

FIG. 1: (Color online) Hugoniot curve computed by QMD simulations (red line) are compared with previous results. Underground nuclear explosive experiments by Nellis *et al.* [7] and Ragan III [6] are labeled as open square and triangle. High power laser results by Cauble *et al.* [8] are shown as open circles. SESAME [9] and multi-phase EOS [24] are shown as dashed and dotted lines, respectively.

The Hugoniot curve is shown in Fig. 1, where previous theoretical and experimental results are also provided for comparison. In the warm dense region, the nature of the continuous transition from condensed matter to dense plasma remains an outstanding and interesting issue in high-pressure physics. One way to address this issue is to measure EOS in the range of 0.1 to 5 TPa. The high shock pressures required to span this range have been reached traditionally with strong shock waves generated by underground nuclear explosives [6, 7], then accessed by high intensity lasers [8]. Good agreement is found from Fig. Fig. 1 between our QMD-determined EOS and those obtained experimentally. The present QMD

EOS indicates a smooth transition from condensed matter to plasma at temperatures from 1.0 eV to 10.0 eV, where we do not find any signs that suggest a first order plasma phase transition. Theoretically, SEMASE EOS [9] also shows an overall accordance with our results. On the contrast, the Hugoniot curve by multi-phase EOS is soften at $\rho \sim 6$ g/cm^3, which corresponds to the imperfect join between the mixed theoretical models [24].

B. Diffusion and viscosity

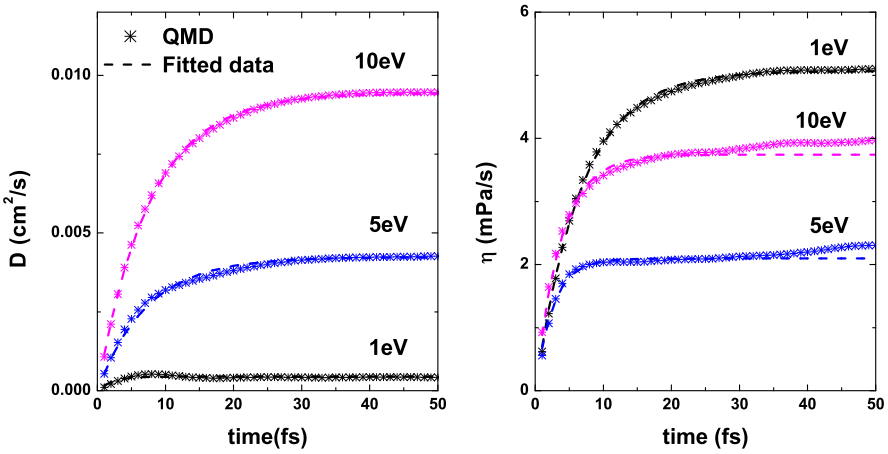

FIG. 2: (Color online) Self-diffusion coefficient and viscosity as a function of time at a density of 5.0 g/cm^3 and different temperatures of 1.0, 5.0, and 10 eV. The fits (dashed lines) are performed for a sample window of [0,4τ-5τ].

We have performed *ab initio* quantum-mechanical simulations with the FT-DFT method to benchmark the dynamic properties of Be in the WDM regime. An example of the QMD results for the self-diffusion coefficient and viscosity of 5.0 g/cm^3 at temperatures of 1.0, 5.0, and 10.0 eV are displayed with their fits in Fig. 2. The current simulations have the trajectory of 10∼20 ps and correlation times between 100 and 200 fs. The computed error lies within 10% for the viscosity. Due to the fitting procedure and extrapolation to infinite time a total uncertainty of ∼20% is estimated by experience. Since the particle average gives an additional $\frac{1}{\sqrt{N}}$ advantage, the error in the self-diffusion coefficient is less than 1%.

Idealized model, such as one-component plasma (OCP) model, concerns the interaction through the Coulomb potential within a neutralizing background of electrons. A large amount of molecular dynamics and Monte Carlo simulations based on OCP model [25–30]

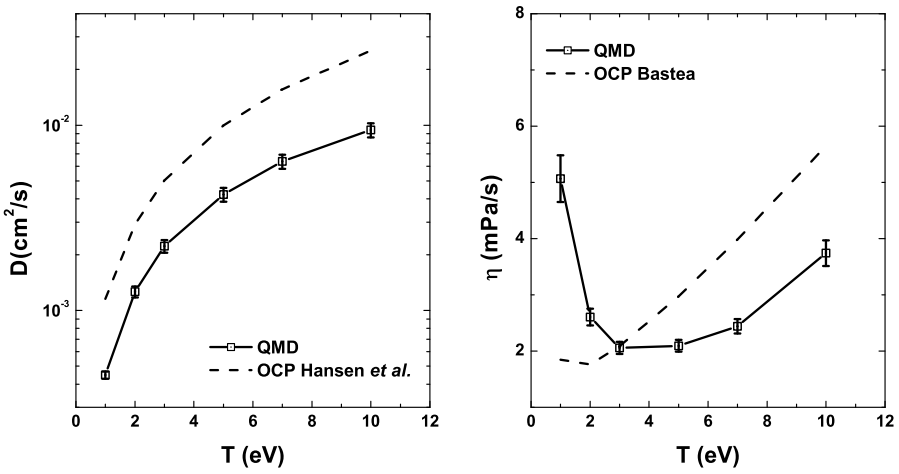

FIG. 3: (Color online) Self-diffusion coefficient (left panel) and viscosity (right panel) as a function of temperature at a density of 5.0 g/cm^3. Only statistical error has been considered here.

have demonstrated that physical properties like diffusion and viscosity can be represented in terms of coupling coefficient, which is defined by the ratio of the potential to kinetic energy:

$$\Gamma = \frac{Z^2 e^2}{a k_B T}, \tag{13}$$

where Ze is the ion charge, and $a = (3/4\pi n_i)^{1/3}$ is the ion-sphere radius with $n_i = \rho/M$ the number density. A memory-function has been used by Hansen *et al.* [30] to analyze the velocity autocorrelation function to obtain the diffusion coefficient for the classical OCP:

$$\frac{D}{\omega_p a^2} = 2.95\Gamma^{-1.34}, \tag{14}$$

with $\omega_p = (4\pi n_i/M)^{1/2} Ze$ being the ion plasma frequency.

Bastea [25] has performed classical molecular-dynamics simulations of the OCP and fits his results to the form

$$\frac{\eta}{n_i M \omega_p a^2} = A\Gamma^{-2} + B\Gamma^{-s} + C\Gamma, \tag{15}$$

with $s = 0.878$, $A = 0.482$, $B = 0.629$, and $C = 0.00188$. As the OCP model is restricted to a fully ionized plasma, determination of the ionization degree for WDM permits an extension of the OCP formulas to cooler systems. A reasonable choice is to replace Z in Eq. (13) with an effective charge $\bar{Z}$. As a consequence, we have introduced average-atom (AA) model [31], which solves the Hartree-Fock-Slater equation in a self-consistent field approximation assuming a finite temperature. In the densities and temperatures we explore, the effective charge $\bar{Z}$ is 2.0, which corresponds to the case of full ionization of the $2s$ electrons.

QMD and OCP results for the self-diffusion coefficient, at the density of 5.0 g/cm^3, are shown in the left panel in Fig. 3. The tendency for the self-diffusion coefficient with respect to temperature is similar for QMD simulations and OCP model. However, OCP model predicts a larger value of the diffusion coefficient compared to QMD results (∼1.5 times bigger). Results for the viscosity, which consists contribution from interatomic potential and kinetic motion of particles, are plotted in the right panel of Fig. 3. The minimum of viscosity along temperature can be attribute to a combined effect, that is, contribution from interatomic potential decreases with temperature, while contribution from kinetic motion increases with temperature. OCP model indicates the local minimum around 2.0 eV, and QMD suggests the location around 3.0 eV.

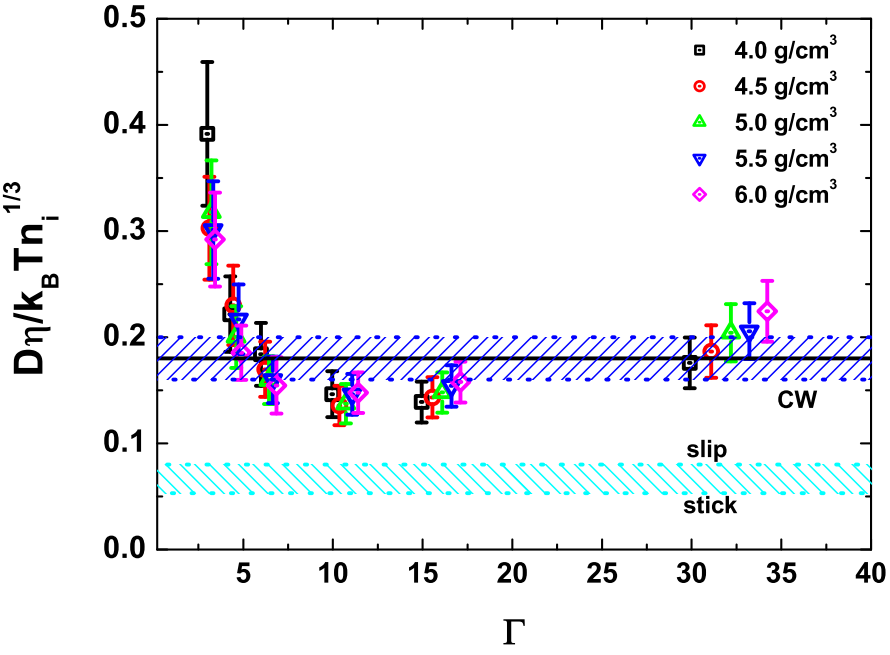

FIG. 4: (Color online) Examination of the Stokes-Einstein relation along the coupling parameter in the warm dense region. Predictions by Chisolm and Wallace [33] are shown as blue region and denoted as 'CW' in the figure. The flat cyan lines show the constant values of C_{SE} for stick and slip boundary conditions [34, 35].

The Stokes-Einstein relation gives a connection between the diffusion and shear viscosity:

$$F_{SE}[D,\eta] = \frac{D\eta}{k_B T n_i^{1/3}} = C_{SE}, \tag{16}$$

where F_{SE} is a shorthand notation for the relationship between the transport coefficients and C_{SE} is a constant. Several prescriptions [32] for determining C_{SE} are available. Chisolm

and Wallace [33] have provided an empirical value of 0.18 ± 0.02 from a theory of liquids near melting. On the other hand, C_{SE}, which has been derived based on the motion of a test particle through a solvent, was assumed to range from $1/6\pi$ [34] to $1/4\pi$ [35] depending on the limits of the slip coefficient from infinity (stick) to zero (slip). Here, we have examined the behavior of Be over the various regimes we explore. As shown in Fig. 4, we have plotted the Stokes-Einstein expression $F_{SE}(D, \eta)$ as a function of the coupling parameter Γ using the diffusion coefficients and viscosities from QMD simulations at densities of 4 $\sim$ 6 g/cm^3 and temperatures from 1 $\sim$ 10 eV. As the expected fitting error of $\sim$ 20% for the viscosity, the QMD results are bounded by the classical values of C_{SE} from below (slip limit) and the Chisolm-Wallace liquid metal value from above at temperatures below 7.0 eV (corresponding to $\Gamma > 4.0$). The function $F_{SE}[D, \eta]$ at the higher temperature evinces a sharp increase with temperature. The near-linear rise of the diffusion coefficient with temperature in the whole region basically cancels the temperature dependence of the denominator. As a consequence, the behavior of $F_{SE}[D, \eta]$ is dominated by the viscosity, which rises sharply at high temperatures as shown in Fig. 3. As mentioned above, this abrupt bend in the viscosity with temperature reflects a change from potential to kinetics dominated regimes.

C. Lorenz Number

We have also computed the Lorenz number defined as

$$L = \frac{K}{\sigma T} = \gamma \frac{e^2}{k_B^2}, \tag{17}$$

where K and σ are the thermal and electrical conductivities, respectively. γ depends on the screened potential and corresponds to the scattering of the electrons [23]. In a degenerate ($\theta \leq 1$) and coupled plasma ($\Gamma \geq 1$), L or γ is a constant ($\pi^2/3$), reaching the ideal Sommerfeld number, which is the value valid for metals, and the Wiedemann-Franz law is recovered in an elastically interacting electron system. As temperature is very high, the WDM enters into a nondegenerate case ($\theta \gg 1$ and $\Gamma \ll 1$), the Lorenz number reaches the value of kinetic matter (4 or 1.5966 depending on the e-e collisions). In the intermediate region, no assumptions can be found for predicting the Lorenz number and one cannot deduce the thermal conductivity from the electrical conductivity by using Wiedemann-Franz law.

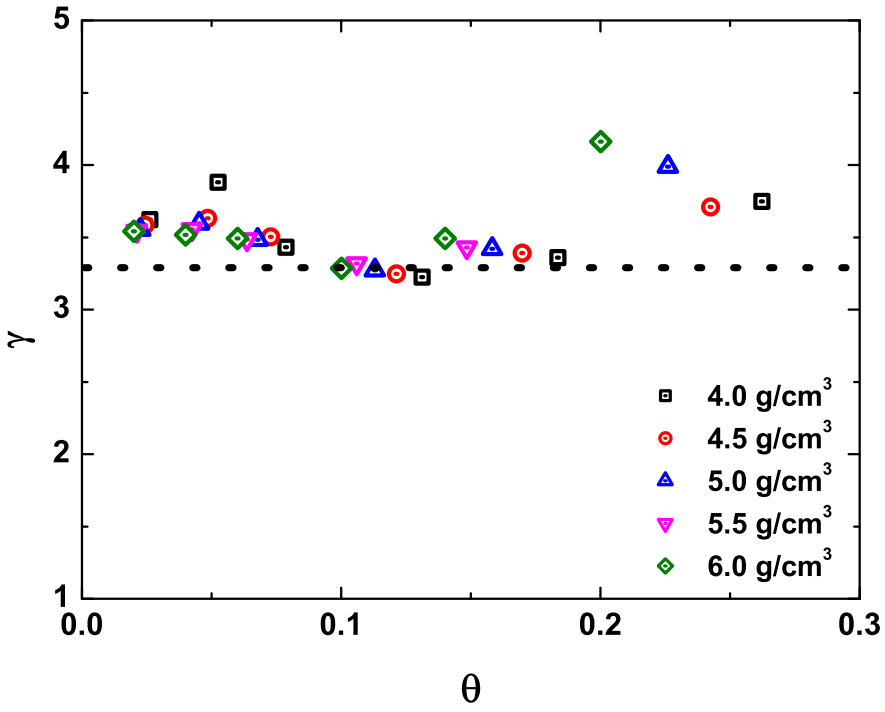

FIG. 5: (Color online) Calculated Lorenz number γ as a function of degenerate parameter θ. The ideal Sommerfeld number is plotted as dotted line in the figure.

In Fig. 5 we show the behavior of γ as a function of the degeneracy parameter θ ($\theta = k_B T/E_F$, with Fermi energy $E_F = \hbar^2 \frac{(3\pi^2 n_e)^{2/3}}{2m_e}$ and electron density n_e). Here, we should stress that in QMD simulations, the electrical conductivity σ and electronic thermal conductance K can be directly evaluated without using any assumption of Lorenz number, which is highly dependent on the two non-dimensional parameters θ and Γ. In the present warm dense regime, the Lorenz number vibrates around the Sommerfeld limit at low temperatures, and as θ increases, a departure of the Lorenz number from the ideal value can be observed from Fig. 5.

IV. CONCLUSION

In the present work, clear chains have been demonstrated in investigating the thermophysical properties of warm dense Be. The EOS has been calculated through *ab initio* molecular dynamic simulations, and smooth functions have been constructed to fit the QMD wide range EOS data, which show good agreement with the underground nuclear explosive

and high pulsed laser experimental results. Based on Green-Kubo relation, the self-diffusion coefficients and viscosity have then been determined, and as a reference, OCP model with an effective charge determined from the average-atom model has also been employed. A Stokes-Einstein relation between the viscosity and diffusion coefficient holds the general feature of liquids as predicted by Chisolm and Wallace in the strong coupling region ($\Gamma > 4$), while, a sharp increase has been observed as temperature arises. The Kubo-Greenwood formula provides an efficient way to study the electrical conductivity and electronic heat conductance in the warm dense regime. Through QMD simulations we have showed that the Wiedemann-Franz law is satisfied for the degenerate regime. Our present results are expected to shed light on the hydrodynamic modeling of target implosions in ICF design.

Acknowledgments

This work was supported by NSFC under Grants No.11275032, No. 11005012, and No. 51071032, by the National Basic Security Research Program of China, and by the National High-Tech ICF Committee of China.

---

[1] D. Saumon, G. Chabrier, and H. M. Van Horn, Astrophys. J. Suppl. Ser. **99** 713 (1995).

[2] S. Atzeni and J. Meyer-ter-Vehn, *The Physics of Inertial Fusion: Beam Plasma Interaction, Hydrodynamics, Hot Dense Matter*, International Series of Monographs on Physics (Clarendon Press, Oxford, 2004).

[3] J. D. Lindl, *Inertial Confinement Fusion: The Quest for Ignition and Energy Gain Using Indirect Drive*, (Springer-Verlag, New York, 1998).

[4] V. E. Fortov *et al.*, Phys. Rev. Lett. **99**, 185001 (2007).

[5] J. D. Lindl, P. Amendt, R. L. Berger, S. G. Glendinning, S. H. Glenzer, S. W. Haan, R. L. Kauffman, O. L. Landen, and L. J. Suter, Phys. Plasmas **11**, 339 (2004).

[6] C. E. Ragan III, Phys. Rev. A **25**, 3360 (1982).

[7] W. J. Nellis, J. A. Moriarty, A. C. Mitchell, and N. C. Holmes, J. Appl. Phys. **82**, 2225 (1997).

[8] R. Cauble, T. S. Perry, D. R. Bach, K. S. Budil, B. A. Hammel, G. W. Collins, D. M. Gold, J. Dunn, P. Celliers, L. B. Da Silva, M. E. Foord, R. J. Wallace, R. E. Stewart, and N. C.

Woolsey, Phys. Rev. Lett. **80**, 1248 (1998).

[9] S. P. Lyon and J. D. Johnson, Los Alamos National Laboratory Report No. LA-UR-92-3407 (1992).

[10] H. F. Robey, Y. Zhou, A. C. Buckingham, P. Keiter, B. A. Remington, and R. P. Drake, Phys. Plasmas **10**, 614 (2003).

[11] R. Betti, V. N. Goncharov, R. L. McCrory, and C. P. Verdon, Phys. Plasmas **5**, 1446 (1998).

[12] B. A. Hammel, M. J. Edwards, S.W. Haan, M. M. Marinak, M. Patel, H. Robey, and J. Salmonson, J. Phys. Conf. Ser. **112**, 022007 (2008).

[13] W. Seka et al., Phys. Plasmas **15**, 056312 (2008).

[14] T. R. Boehly et al., Phys. Plasmas **13**, 056303 (2006).

[15] V. Bezkrovniy, V. S. Filinov, D. Kremp, M. Bonitz, M. Schlanges, W. D. Kraeft, P. R. Levashov, and V. E. Fortov, Phys. Rev. E **70**, 057401 (2004).

[16] T. Lenosky, S. Bickham, J. Kress, and L. Collins, Phys. Rev. B **61**, 0163 (2000).

[17] G. Kresse and J. Hafner, Phys. Rev. B **47**, R558 (1993).

[18] G. Kresse and J. Furthmüller, Phys. Rev. B **54**, 11169 (1996).

[19] P. H. Hünenberger, Adv. Polym. Sci. **173**, 105 (2005); D. J. Evans and B. L. Holian, J. Chem. Phys. **83**, 4069 (1985).

[20] M. P. Allen and D. J. Tildesley, *Computer Simulation of Liquids* (Oxford University Press, New York, 1987).

[21] J. D. Kress, James S. Cohen, D. P. Kilcrease, D. A. Horner, and L. A. Collins, Phys. Rev. E **83**, 026404 (2011).

[22] R. Zwanzig and N. K. Ailawadi, Phys. Rev. **182**, 280 (1969).

[23] G.V. Chester and A. Thellung, Proc. Phys. Soc. (London) **77**, 1005 (1961).

[24] L. X. Benedict, T. Ogitsu, A. Trave, C. J. Wu, P. A. Sterne, and E. Schwegler, Phys. Rev. B **79**, 064106 (2009).

[25] S. Bastea, Phys. Rev. E **71**, 056405 (2005).

[26] F. Lambert, Ph.D. thesis, Université Paris XICCommissariatà l' Énergie Atomique, 2007.

[27] B. Bernu and P. Vieillefosse, Phys. Rev. A **18**, 2345 (1978).

[28] Z. Donkó, B. Nyíri, L. Szalai, and S. Holló, Phys. Rev. Lett. **81**, 1622 (1998); Z. Donkó and B. Nyíri, Phys. Plasmas **7**, 45 (2000).

[29] J. Daligault,Phys. Rev. Lett. **96**, 065003 (2006); **103**, 029901(E) (2009).

[30] J. P. Hansen, I. R. McDonald, and E. L. Pollock, Phys. Rev. A **11**, 1025 (1975).

[31] B. F. Rozsnyai, Phys. Rev. A **5**, 1137 (1972).

[32] M. Cappelezzo, C. A. Capellari, S. H. Pezzin, and A. F. Coehlo, J. Chem. Phys. **126**, 224516 (2007).

[33] E. Chisolm and D. Wallace, *Shock Compression of Condensed Matter*-2005, AIP Conf. Proc. No. 845, edited by M. D. Furnish, M. Elert, T. P. Russell, and C. T. White (AIP, New York, 2006).

[34] A. Einstein, Z. Elektrochem. **14**, 235 (1908).

[35] W. Sutherland, Philos. Mag. **9**, 781 (1905).